CFD modelling of a pallet of heat-generating product applied to a cheese product

Anh Thu Pham, Jean Moureh, Mourad Belaidi, Denis Flick

CFD modelling of a pallet of heat-generating product applied to a cheese product

Anh Thu Pham [(1)(2)(3)], Jean Moureh [(1)(*)],Mourad Belaidi [(1)], Denis Flick [(2)]

(1) Inrae, UR FRISE, Refrigeration Process Engineering Research Unit, 1 rue Pierre-Gilles de Gennes, F-92761 Antony, France

(2) AgroParisTech, Inrae, Université Paris-Saclay, UMR Ingénierie Procédés Aliments, 1 Rue des Olympiades, 91300 Massy, France

(3) CNIEL, 42, rue de Châteaudun – 75314 Paris Cedex 9, France

(*)corresponding author's address:

Food Process Engineering, Irstea, 1 rue Pierre-Gilles de Gennes, CS 10030, 92761 Antony Cedex, France

e-mail: jean.moureh@inrae.fr

Tél. (direct): +33 (0)1 40 96 60 88

Tel.(operator): +33 (0)1 40 96 61 21

Fax : +33 (0)1 40 96 62 49

Abstract

This work aimed to numerically study the heat transfer and airflow within a pallet of heat-generating product. A computational fluid dynamics (CFD) model of palletized cheese inside a cold room was developed. The model took into account the effect of natural convection induced by the heat-generating product. A full-scale experimental set-up under controlled operating conditions was built to validate the model. The air velocity within the pallet was measured using Laser Doppler Velocimetry (LDV). Three heat fluxes and two upwind air velocities were chosen: Q = 0.05W, 0.15W and 0.30W per product with a mass of 250g; $u_{air.in}$ = 0.31m.s^{-1} and 0.73m.s^{-1}. The model predicted well both the product temperatures and airflow patterns. This model is a potential design tool to be used to optimize the cooling system of a heat-generating product. The model can also be adapted for other food products as well as other types of packaging.

Keywords: Heat transfer, temperature distribution, cheese, heat-generating product, airflow pattern

NOMENCLATURE

D	Cheese diameter	[m]
g	Acceleration due to gravity	[m.s^{-2}]
Q	Heat flow per product item	[W]
T	Temperature	[K]
u	Flow velocity	[m.s^{-1}]

Greek symbols

ΔT	Temperature difference: T-$T_{a.in}$	[K]
β	Thermal expansion coefficient	[K^{-1}]
λ	Thermal conductivity	[W.m^{-1}.K^{-1}]
ρ	Density	[kg.m^{-3}]
ν	Kinematic viscosity	[m^2.s^{-1}]
k	Turbulence kinetic energy	[m^2. s^{-2}]
ε	Turbulence dissipation rate	[m^2. s^{-3}]

Dimensionless numbers

Nu	Nusselt number	[-]
Gr	Grashof number	[-]
Pr	Prandtl number	[-]
Re	Reynolds number	[-]
Ri	Richardson number	[-]

Indices

a	air
in	inflow/ upwind
p	product

1 Introduction

Temperature is the most important factor to be taken into consideration when ensuring the quality of a product throughout the cold chain (Ambaw et al. 2016; Defraeye et al. 2015). The temperature evolution depends greatly on the air flow within the pallets. Moureh and Flick (2004) and Moureh et al. (2002) pointed out that the compactness of the pallets increases the heterogeneity of ventilation. Moureh et al. (2009) showed that in the same enclosure, the rear pallet was 20 times less ventilated than the front pallet. Cooling heterogeneity exists also within the pallet (Hoang et al. 2012).

A constant uniform temperature is difficult to obtain for stacked food products in general, and is even more challenging for heat-generating products such as cheese. Leclercq-Perlat et al. (2015) showed that an increase in temperature induces microorganisms growth. This results in the change in the quality of the product (color, texture and odor). For example, the authors indicated that the color of the Camembert can change from white at 8°C to brown at 16°C.

Air distribution is one of the most important factors to be taken into consideration when ensuring the level and the uniformity of cooling. In cold chain facilities, cheese is often packed in vented cardboard boxes which are then stacked on pallets. An optimal ventilation system associated with a suitable vented package design should promote internal ventilation within the pallet. This allows cold air to flow within and around the packed product and enables evacuation of warm air.

The heat generated by the product induces natural convection while the airflow is dominated by forced flow around the pallet. Therefore, a mixed convection regime can occur within the pallet. The airflow and heat transfer within a stack of product have been studied numerically by many authors. Different parameters have been taken into account: packaging material (Ngcobo et al., 2012), package vents (Defraeye et al., 2014; Ferrua and Sing, 2009; Castro et al., 2004), stacking pattern (Ferrua and Sing, 2009), and airflow rate (Tutar et al., 2009). However, none of these studies took into account the effect of the respiration heat of the product. The assumption that heat generation is a negligible factor is commonly made (Ferrua and Sing, 2008; Defraeye et al., 2013). It was claimed to have an insignificant impact on the cooling rate of fresh horticultural produce during forced-convective precooling (Sadashive Gowda et al. 1997). However, mixed convection can occur during the storage of heat-generating products because of poor ventilation.

The mixed convection regime is rarely studied in the case of stacked food products. However, mixed convection can be found in many other fields such as solar collectors, ventilation of electronic devices, compact heat exchangers and nuclear reactors (Tian et al., 2018).

The presence of natural convection can create recirculating zones between the products (Boutina and Bessaïh, 2011) and reverse flow (Maré et al., 2005).These two phenomena were found to play an important role in heat transfer (Tian et al., 2018; Boutina and Bessaïh, 2011). The occurrence of mixed convection can be determined by the combination of the Reynolds, Grashof and the Prandtl numbers (Maré et al., 2005). The recirculating zones decrease when the Reynolds number increases and the heat flux decreases (Boutina and Bessaïh, 2011). The most common criterion used to determine the mode of convection is the Richardson number (Gr/Re2) which represents the ratio between the buoyancy and the inertial forces. When $Ri < 0.1$, natural convection is negligible; when $Ri > 10$, forced convection is negligible, and mixed convection occurs when $0.1 < Ri < 10$ (Tian et al.,

2018). However, in some cases such as non-uniform heat flux (Huang et al., 2017), inclined and narrow rectangular channels (Tian et al., 2018), mixed convection cannot be determined by the Richardson number alone.

Forced flow and flow induced by natural convection can be in the same direction (enhancing mixed convection), opposing directions (opposing mixed convection) or perpendicular (transverse mixed convection) (Sumon et al., 2016). Depending on the system, free convection can promote or prevent heat transfer. Joye (1996) found that an opposing direction gives better overall heat transfer than assisting direction. While studying heat transfer inside a horizontal circular cylinder, Mohammed and Salman (2007a) concluded that natural convection improves the heat transfer for high Reynolds numbers and decreases heat transfer where Reynolds numbers are low. Transverse mixed convection allows better mixing and a higher heat transfer coefficient (Tian et al., 2018). Since the position of natural convection flow with respect to forced flow greatly influences heat transfer, a number of authors have chosen to study the angle of the heating surface (Boutina and Bessaïh, 2011; Chong et al. 2008; Maughan and Incropera, 1987). Mohammed and Salman (2007b) found that at low Reynolds numbers, the Nusselt number increased as the cylinder moved towards the horizontal position. While at high Reynolds numbers, the Nusselt number increased as the angle of inclination moves towards 60°. These studies proved that the inclination angle of the heating surface is not the only parameter that influences heat transfer under mixed convection. The Nusselt number can increase or decrease with the increase in the inclination angle under different conditions (Chong et al., 2008).

The geometrical parameters of the system also play an important role in heat transfer. Boutina and Bessaïh (2011) found that heat transfer increases when the dimensions of the heat source increase compared with the height of the channel. Also, when the distance between the heat sources is increased, the average Nusselt number rises (Ali et al., 2018).

The increasing development of both computers and the field of computational fluid dynamics (CFD) in recent years has opened up possibilities to perform numerical modelling and simulations with an acceptable level of accuracy and with fewer experiments required. This makes it possible to obtain a complete description of the three-dimensional flow in the entire system in terms of velocity field and temperature distribution.

To take into account the effect of products on the airflow within the stack, numerous studies (Moureh et al., 2009; Van der Sman, 2002; Zou et al. 2006; Delele et al., 2013) used the porous-medium approach since it is easy to implement in the numerical model. This two-phase approach eliminates the need to generate complicated meshes to describe the geometric details of individual products in terms of size, shape, and air gap spaces within the load. However, the continuous-medium assumption becomes questionable, especially when the ratio of package-to-produce diameter is less than 10 (Whitaker, 1986), which often occurs in the case of individual packages of cheese. In these cases, the heterogeneity of the local airflow pattern within packages exerts a major impact on the transport phenomena (Ferrua and Singh, 2008). Another significant limitation of this approach is that it neglects internal product gradients and the inertial effects of airflow around vents (Zhao et al. 2016).

To overcome the limitations of the porous-medium approach, direct CFD simulations based on the explicit geometry of produce and ventilated boxes were developed to investigate the airflow and

temperature distribution within stacks of horticultural products. Despite the greater computational requirements and numerical difficulties, direct CFD simulations lead to a more fundamental understanding of the local behavior of the fluid flow and heat transfer within packages.

Zhao et al. (2016) and Ambaw et al. (2013) reviewed the application of CFD to analyze forced convection cooling of horticultural products and confirmed the value of CFD as an efficient tool for modelling of transport phenomena inside complex packaging.

Zhao et al. (2016) recommend the use of the porous medium approach for large spaces (such as a cold room, a refrigerated vehicle, refrigerated containers) in order to understand the macro phenomena of spatiotemporal heat and mass transfer, and direct CFD simulations for small ensembles of packages to obtain the detailed characteristics of the airflow and heat transfer [32-34].

Geometric modeling and grid generation become complicated because of the explicit geometry of the produce included in direct CFD simulations, which increases the computational requirements and numerical difficulties. However, the method can lead to a more fundamental understanding of how local behavior of the fluid flow affects the heat and mass-transfer processes within the packaging of various fresh produce during cooling. This method is more significant than the porous-medium approach for improving the design of packaging systems and their stacking pattern on the pallet.

Depending on industrial applications, CFD models are used to identify local airflow characteristics as a function on ventilated package design (Defraeye et al., 2013; Wu et al., 2019, Getahun et al., 2017) , their stacking pattern on a pallet (Wu and Defraeye, 2018), pallet arrangement (Sajadiye and Zolfaghari, 2017) or cold chain scenarios (Wu and Defraeye, 2018; Wu et al., 2019).

Defraeye et al. (2013) evaluated the cooling performance of three types of citrus packages, where all stacked packages were filled using real citrus fruit. There was an underestimation of the predicted cooling rate. The possible cause of this underestimation was reported as imperfect stacking during the experiment that could increase the airflow through the vents, but the model assumed perfect stacking.

Wu and Defraeye (2018) used the virtual cold chain method to study the heterogeneity in cooling and quality evolution of packed fresh fruit in a pallet for three cold chain scenarios. The pallet includes 80 cartons, in which 5120 fruit are explicitly modelled as discrete spheres. The results show that regular stacking pattern on a pallet leads to a periodical airflow patterns between different layers. However, in the case of a more complicated carton stacking, as in practice, would cause partial blockage of vent holes on the interface of different layers and might introduce more heterogeneity in airflow distribution. For all the three unit operations in a cold chain (precooling, transport and storage), significant differences in the fruit cooling time are found along the airflow direction, where the blockage of local vent holes is found to increase the thermal heterogeneity. Fruit in upstream cartons also show a higher cooling heterogeneity than those in downstream cartons.

Wu et al. (2019) investigate the effect of package design its positioning on a pallet, package stacking pattern but also cold chain scenario on the remaining fruit storage life of a complete pallet of fruit, and the related heterogeneities within the pallet. Comparisons between the three packaging designs show that unequal distribution of the vent openings on the long and short sides creates preferential

pathways, causing non-uniform fruit cooling times and the fact that these openings were located at the top of the package, leads to a preferential cooling of the top layer of fruit. The results also show that stacking the pallet in a mechanically more stable way negatively affects the cooling heterogeneity.

Getahun et al. (2017) used a validated CFD model to compute the aerodynamic and thermodynamic characteristics of three package designs. The effects of vertical flow resistance on the rate and uniformity of cooling was investigated. The study demonstrated the significance of vent-holes on the bottom face of packaging boxes and the potential energy saving opportunities in refrigerated transport systems. Adding vent-holes (3.5% vent area) on the bottom face of the package reduced vertical airflow resistance, and reduced the seveneighth cooling time by 37% compared to a package with no bottom vent-holes.

Han et al. (2018) develop a computational fluid dynamics (CFD) model based on the explicit geometry of produce stacked in boxes was used to study to evaluate the cooling rate, uniformity, moisture loss, and energy consumption for palletized apple packages. Buoyancy effects and radiation were assumed negligible and not taken into account in the simulations. Numerical results show that maintaining lateral vent holes allow to decrease the cooling time by 14.5% for downstream boxes. Also, cold-air exchange between stacked boxes through lateral vent holes contributes to uniform temperature distribution by 10% throughout the pallet layer. Additionally, the cooling rate of fruit did not significantly improve when the pressure drop exceeded 600 Pa or 0.83m/s for superficial velocity.

Despite all the above-mentioned advantages and encouraging numerical results, the accuracy and reliability of CFD simulations remain important concerns and therefore, CFD validation and verification are imperative. However, it is noteworthy that the validation of the majority of CFD models reported in the literature (Delele et al., 2008; Dehghannya et al., 2012; Ngcobo et al., 2013) was obtained by using intrusive point wise velocity measurements or indirect techniques such as measurements of pressure drop or temperatures. Thus, there is a need to use more advanced non-intrusive techniques such as LDV in order to obtain sufficiently high resolution to characterize airflow patterns and velocity profiles. The obtaining of such results provides a better understanding of airflow characteristics and also improves the quality of CFD validation.

Although many aspects of heat transfer under mixed convection have been studied, no study applied to palletized food product was identified. This study aimed to predict heat transfer and airflow within a pallet of heat-generating product (cheese) by direct three-dimensional CFD modelling. The model took into account the detailed geometries of the products and of the boxes (size, shape and location of vent holes) as well as the heat generated by the respiration of the product. The aim was to gain a better insight into the effect of all these parameters on the local heterogeneities of velocities and temperatures within the packages. Finally, validation of the model was obtained by comparisons with experimental data related to velocities obtained by LDV and temperature measurements. These aspects are deeply investigated in our previous papers related to the same configuration (Pham et al., 2019).

2 Materials and method

2.1 Experimental set-up

The experimental pallet described by Pham et al. (2019) consisted of 9 layers of boxes. Each layer contained 6 boxes, and 30 products per box. In order to ensure reproducible experiments, cheese was replaced by plaster blocks in which heating resistances were inserted in order to simulate the heat flux of the product. The pallet was placed inside a room with controlled temperature and upwind air velocity (Figure 1). The upwind air velocity in the experimental room varied between 0.31m.s^{-1} and 0.73m.s^{-1}.

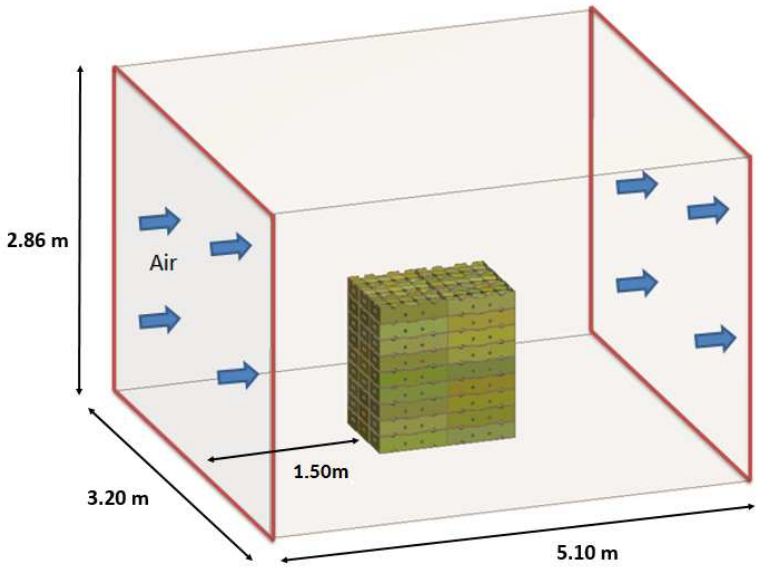

Figure 1. Simplified diagram of the room in which the experimental work was conducted

2.1.1 Temperature measurement

The temperature was measured using T-type thermocouples (with a precision of ±0.1 *K* after individual calibration between 273 and 293 *K*). The product temperatures were measured on the axis of the cylindrical small blocks, 5 mm from the top. Even the temperature in the test room was controlled at 4 °C, the real air ambient temperature varied slightly.

2.1.2 LDV measurement

The air velocity within the pallet was measured using LDV. The LDV device (Dantec FlowExplorer-2D) is composed of two 70 mW laser diodes emitting two laser beams at 660 nm and 785 nm, a Bragg cell, a focusing and receiving lens, a beam splitter, a photomultiplier and a pinhole arrangement to collect scattered light. The accuracy of LDV is estimated to be less than 1% for velocity measurement of one tracer particle (manufacturer's data) and better than 2.3% for the time-averaged velocity. The LDV was placed on a displacement system that makes it possible to control movement in three directions (x, y, z). The movement of the LDV was controlled by a computer placed outside the experimental room. The number of tracked particles at each measurement point varied between 2000 and 10 000. Since LDV cannot measure directly the air velocity, the presence of microscopic particles in the air is needed. Therefore, an atomizer (manufactured by Areco, reference OD V7) was

used to spread water droplets inside the air stream. These water particles were then conveyed into the pallet by the air stream and allowed LDV measurements when they passed through the laser beams. The mean diameter of the droplets is 7µm, their settling velocity, about 1.5 mm/s, is small compared to the measured velocities.

Due to its low airflow resistance, the headspace (the space between the top of the product in a box and the bottom of the box located above it) which is directly connected to the main vent holes, forms an important internal channel acting as a preferential pathway within a pallet layer. In forced-convection dominating flow, the horizontal headspace flow makes it possible to capture and evacuate the heat generated by the packed products for the considered layer. This ensures internal ventilation while avoiding heat accumulation in the core of the pallet. Figure 2 presents the lines along which the velocity profiles were measured at the mid-height of the headspace.

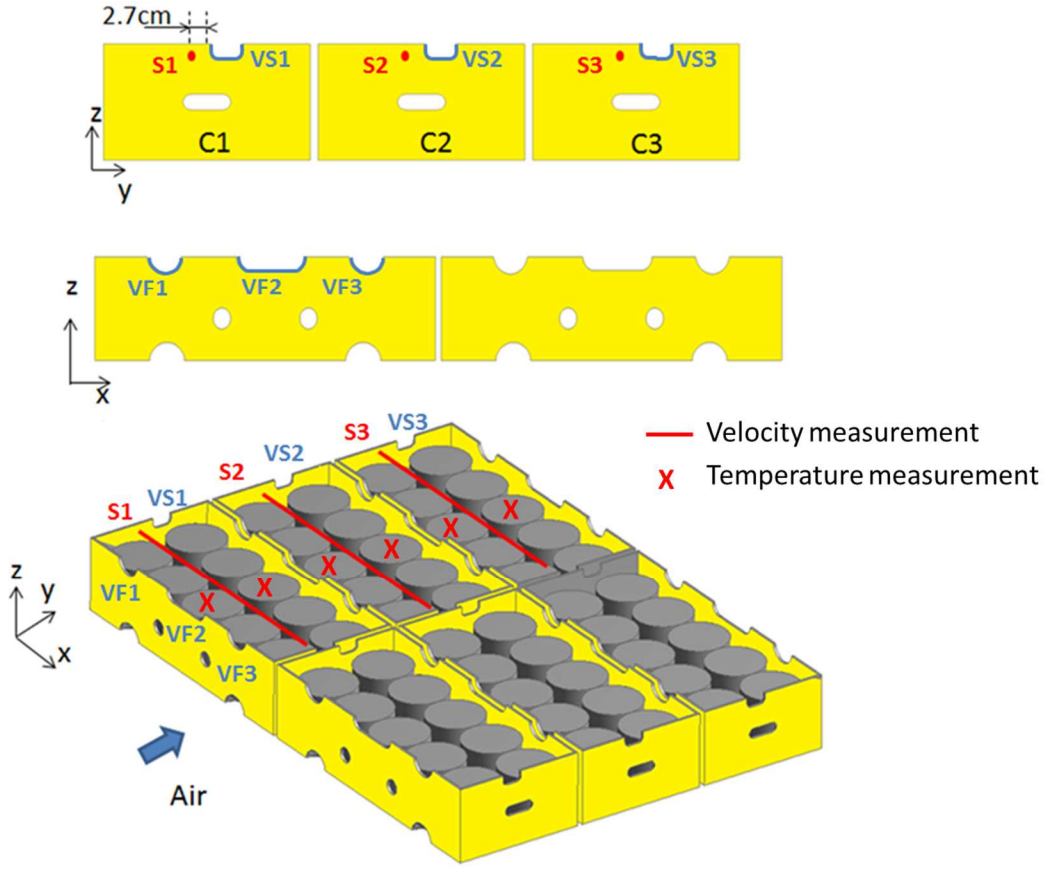

Figure 2. Velocity and temperature profiles used to validate the model

2.1.3 Hot wire anemometer measurements at the vent centers

Due to optical constraints, LDV measurement is not possible on vent sections. Therefore, the authors attempted to estimate the velocity at the center of the vents by using a hot wire anemometer (Testo 435-4). The supplier specified that the precision is 5% of the read value or ±0.03 $m.s^{-1}$. These measurements are difficult because positioning the sensor exactly in the center of the vent hole is difficult and the sensor can disturb the flow. In addition, flow is not necessarily normal to the vent section. Also, it can be difficult to define the actual direction of flow for certain vents located in low-velocity areas subjected to thermal instabilities. Nevertheless, an order of magnitude of velocity can

be obtained, making it possible to estimate the corresponding airflow rate from the cross-sectional area.

The hot wire anemometer was positioned to measure the component of the velocity which is perpendicular to the vent hole. Each measurement was performed twice, and the mean value of these two measurements was used. The velocities at both the left and right sides of the pallet were measured. Since the pallet is quasi-symmetrical, only half of the pallet is presented with the mean value of the left and right sides. The difference between the left and right measurements was about 14%.

2.1.4 Experimental conditions

The fan speed was adjusted to obtain an upwind air velocity of 0.31 $m.s^{-1}$ and 0.73 $m.s^{-1}$.The heat flux generated by the product was varied in order to cover a wide range of Richardson numbers, since the Richardson number characterizes mixed convection. For this study, the Reynolds, Grashof and Richardson numbers were defined as follows:

$$Re = \frac{u_{air.in} D}{\nu} \quad (1)$$

$$Gr = \frac{g\beta Q D^2}{\lambda \nu^2} \quad (2)$$

$$Ri = \frac{Gr}{Re^2} = \frac{g\beta Q}{\lambda u_{air.in}^2} \quad (3)$$

where D is the diameter of one camembert (110 mm) which is close to the height of three superimposed camemberts with packaging (3x40 mm); $u_{air.in}$ is the upwind velocity and Q is the heat flow corresponding to one camembert; g=9.81 $m.s^{-2}$, ν=1.57*10-5 $m^2.s^{-1}$, λ=0.026 $W.m^{-1}.K^{-1}$, β=0.0036 K^{-1}. In the experiments, the Richardson numbers ranged from 0 to 3.5. The heat flux generated by one camembert with a mass of 250 g was estimated to be about 0.1 W based on the study of Hélias et al. (2008)

Table 1 summarizes the experimental conditions.

Table 1. Test Conditions

	u = 0.31 $m.s^{-1}$ (*Re* = 1541)	*u* = 0.73 $m.s^{-1}$ (*Re* = 4203)
Heat flux (per 250-g cheese item)	0W (*Ri*=0)$^{\Delta}$	0W (*Ri*=0)$^{\Delta}$
	0.05W (*Ri* =0.58) *$^{\Delta}$	0.05W (*Ri*=0.11) *$^{\Delta}$
	0.15W (*Ri*=1.75) *	0.15W (*Ri*=0.32) *
	0.30W (*Ri*=3.51) *$^{\Delta}$	0.30W (*RI* =0.63) *$^{\Delta}$

*Temperature measurements; $^{\Delta}$ Velocity measurements

2.2 CFD model

2.2.1 Geometrical configurations

One pallet contains 1620 camemberts. Due to the limit of the computational resources, it was not possible to model a whole pallet. Also, it was found that there was no significant temperature difference between the 9 layers of the pallet with the exception of the top layer which was in direct contact with ambient air Pham et al. (2019).

Therefore, only the middle box layer of the pallet was modelled, since the most important objective was to identify the maximum temperature of the product. The dimensions of the box are presented by Pham et al. (2019). The model considered cylindrical blocks representing 3 superimposed camemberts. The ratio between the thickness of the cardboard and the vent hole smallest dimension is less than 0.07, the thermal inertia of the cardboard is negligible comparing to the one of the product. Therefore, the thickness of the cardboard was neglected. The camemberts were equidistantly arranged inside the cardboard box. The air gaps between boxes (1 cm) were also modelled.

2.2.2 Hypotheses

In order to reduce the calculation time, several hypotheses were applied to our model:

- The heat exchange by radiation can be neglected in comparison with convection since products which radiate each on the others have approximately the same temperature whereas for convection, product temperature is significantly higher than the air temperature (Pham et al., 2019).. Duret et al. (2014) also found that heat transfer by radiation was negligible while studying the heat transfer in a cold room filled with food products.
  Therefore, the model did not include radiation. Heat transfer by conduction and convection was taken into account. Natural convection was also included in the model by using the ideal gas law and activating gravity
- Each product was packed in primary packaging including stagnant air (Figure 3)
- A source term was defined within the product with constant volumetric heat generation $q=Q/V_p$, where Q is the heat load (W) and V_p the product volume (m^3). The condition volumetric heat source was applied to the product zone. However, it should be reminded that in the real case, heat release mostly on the surface of cheese.

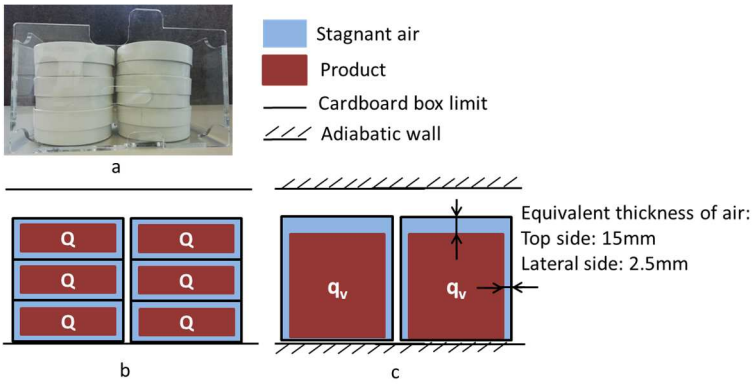

Figure 3 a). Photo of cheese wrapped in the primary packaging; b) simplified diagram showing cheese packaging; c) diagram of the model.

2.2.3 Governing equations

The airflow and heat transfer predictions are based on the conservative laws of mass momentum and energy. They were formulated using the Reynolds-averaged Navier-Stokes equations. The buoyancy effect is included in the momentum equation, and density is treated using the incompressible ideal gas law (density varies with temperature alone).

In this study, the realizable κ-ε turbulence model Shih et al. (1995) with Enhanced Wall Treatment was used. This near-wall modelling method, that combines a two-layer model, guarantees the correct asymptotic behavior for large and small y^+ values and reasonable representation of velocity profiles in the cases where y^+ falls inside the buffer region. This is obtained by blending the linear (viscous-sublayer) and logarithmic (turbulent) laws using a function suggested by Kader (1981).

The κ-ε turbulence model has been chosen in many studies (Ali et al., 2018; O'Sullivan et al., 2016; Park et al., 2018; Asako and Faghri, 1991). Sarper et al. (2018) also claimed that the realizable k-ε is more accurate for modelling flows with recirculation and flow separation. The equations can be written as follows:

Mass conservation:

$$\frac{\partial(\rho u_i)}{\partial x_i} = 0 \tag{4}$$

Momentum conservation:

$$\frac{\partial\left(\rho u_i u_j\right)}{\partial x_j} = -\frac{\partial p}{\partial x_i} + \frac{\partial}{\partial x_j}\left[\mu\left(\frac{\partial u_i}{\partial x_j} - \rho\overline{u_i' u_j'}\right)\right] + \left(\rho - \rho_0\right)g_i \tag{5}$$

Energy conservation:

$$\frac{\partial \rho C_p u_j T}{\partial x_j} = \frac{\partial}{\partial x_j}\left(\lambda\frac{\partial T}{\partial x_j}\right) - \frac{\partial}{\partial x_j}\left(\rho C_p \overline{u_j' T'}\right) \tag{6}$$

where $\overline{u_i' u_j'}$ and $\overline{u_j' T'}$ are, respectively, the unknown Reynolds stresses and turbulent heat fluxes. The obtaining of these quantities depends on the turbulence closure. A common method is to use the Boussinesq hypothesis that relates the Reynolds stresses with mean velocity gradient through eddy viscosity and the turbulent heat fluxes are modelled based on the Boussinesq analogy to turbulent momentum transfer expressed as:

$$-\rho C_p \overline{u_j' T'} = \frac{C_p \mu_t}{\sigma_t}\frac{\partial T}{\partial x_j} \tag{7}$$

where μ_t is the turbulent eddy viscosity, and σ_t is the turbulent Prandtl number.
The realizable k-ε model of Shih et al. (1995) improves the standard k-ε model described by Launder and Spalding (1974) by introducing a new dissipation rate equation model for ε while keeping the same transport equation for turbulent kinetic energy k.

The eddy viscosity formulation is the same as that of the standard k-ε model Eq. (8)

$$\mu_t = \rho C_\mu \frac{k^2}{\varepsilon} \quad (8)$$

To achieve the positivity of normal Reynolds stresses, C_μ is no longer constant but is a function of the turbulence fields, mean strain and rotation rates (Shih et al.,1995).

2.2.4 Computational grid

The space between the products is very narrow (about 1mm), which is less than 1% of the diameter of the product. In certain cases, the contact between the products can cause highly skewed elements which may compromise the convergence of the numerical solution; one solution involves the creation of small gaps to avoid meshing problems. For this purpose, Ferrua and Sing (2009) modelled spheres with a diameter equal to 99% of that of the real ones, O'Sullivan et al. (2016) found that 2mm is the minimum distance between two kiwi fruit that makes it possible to avoid distorted and unstable mesh. Therefore, in our model, the length of the cardboard box was 1cm longer than that of the real one in order to avoid meshing problems.

Due to the complexity of the geometric configuration including rectangular shapes (box, external domain) and circular shapes (vents, products), a hybrid grid combining tetrahedral and hexagonal cells was built within the computational domain.

A coarser mesh was created close to the inlet and outlet boundaries, which became finer near the package domain where high velocity and temperature gradients are expected. The size and density distribution of the mesh were determined to ensure a good mesh in regions where critical features of flow occur such as around the vent holes and within air gaps separating products. Very fine hybrid mesh was also used inside the products to determine the heat transfer. Special care was taken to create a finer mesh around the product walls to accurately capture the interfacial heat fluxes.

Prior to performing numerical model simulations, mesh sensitivity analysis was conducted to determine the most suitable mesh configuration for our model. Different numbers of elements were tested: 5 10^5, 5 10^6, 8 10^6, 10^7 and 1.7 10^7. To examine the reliance of numerical accuracy on grid sizes, the configuration with the highest natural convection effect ($u_{air.in}$ =0.31m.s^{-1} and Q=0.30W) was chosen to compare the results. Figure 4 shows the maximum temperature as a function of the number of elements. It can be seen that from 10^7 elements, the results stabilize. The maximum temperature difference between10^7 and 1.7 10^7 cells is 0.2°C.Also, the difference of the total airflow rate between these two grids at the upstream vent holes is 1.6% and 1.7% for the downstream vent holes. Therefore, it can be considered that increasing the grid number to more than 10^7 does not improve significantly the precision of the result.

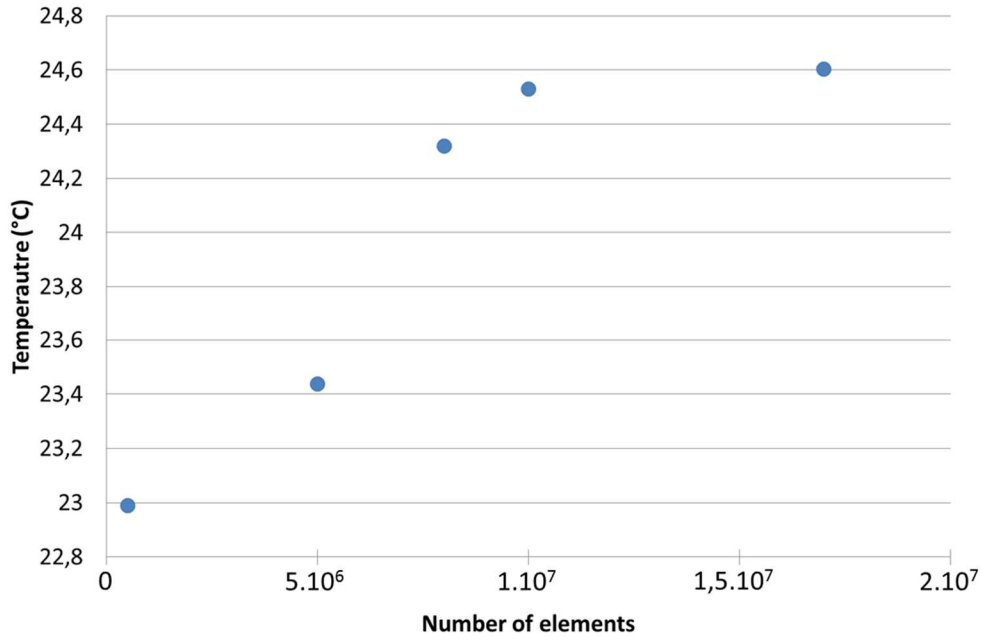

Figure 4. Maximum temperature as a function of the number of elements

2.2.5 Boundary conditions

The boundary conditions applied to the domain are presented in Figure 5.

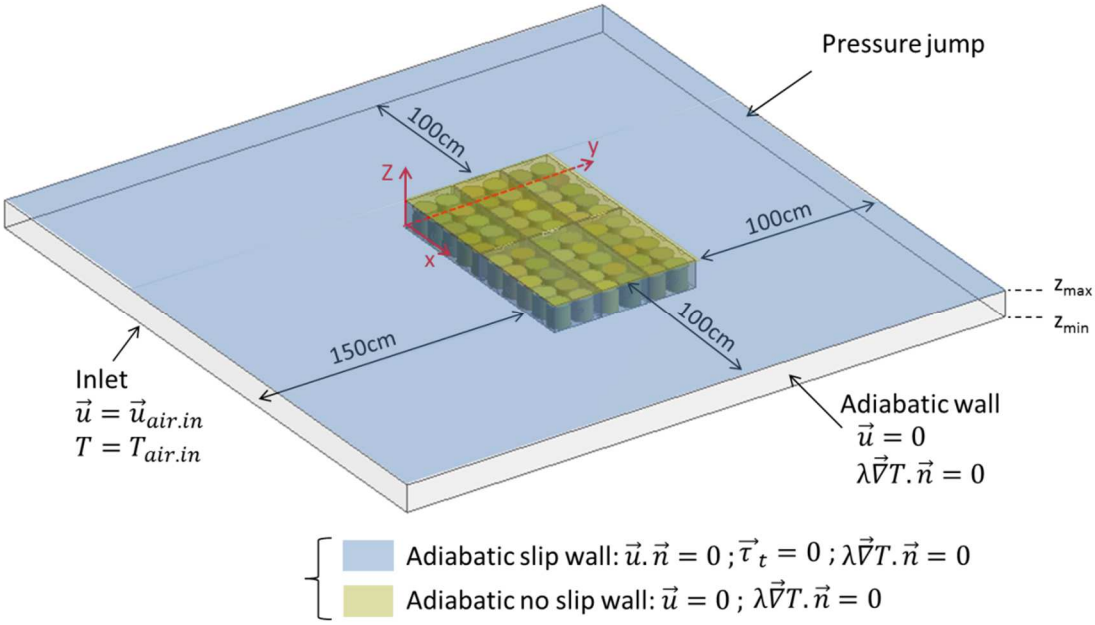

Figure 5. Simulated domain and boundary conditions

The air inflow temperature was set at 4°C. The air inlet and outlet of the experimental room included perforated plates in order to create homogeneous flow. In the model, uniform inlet velocity was assumed and a high pressure drop was applied at the outlet in order to homogenize the flow. The inlet air velocity was0.31 $m.s^{-1}$ and 0.73 $m.s^{-1}$. Three heat fluxes were applied: Q=0.05W, 0.15W, and 0.30W.

2.2.6 Simulation set-up

The geometry realization, domain meshing and numerical simulation were performed by the commercial CFD code ANSYS Fluent 18.1. Pressure interpolation was second order. Second Order Upwind discretization was used for momentum and energy. First Order Upwind discretization was used for turbulent kinetic energy and turbulent dissipation rate.

The simulations were performed on a 64-bit Windows7 computer with a 3.70 GHz Intel® Xeon® CPU E5-1630 v4 and 192 Go (RAM). The calculation time for each simulation was about 48 hours.

3 Results

3.1 Model validation

Validation of the model was performed by comparing the numerical results with the experimental data which included airflow and product temperature measurements (Pham et al., 2019).

3.1.1 Airflow validation

Figure 6 presents the distribution of the airflow rate ($\sum u_{vent} * A_{vent}$) expressed as a percentage of the inflow rate, on each face of the box without heating for two upwind velocities ($u_{air.in}$ =0.31m.s^{-1} and 0.73m.s^{-1}). Each position measurement is the mean value during 1 minute.

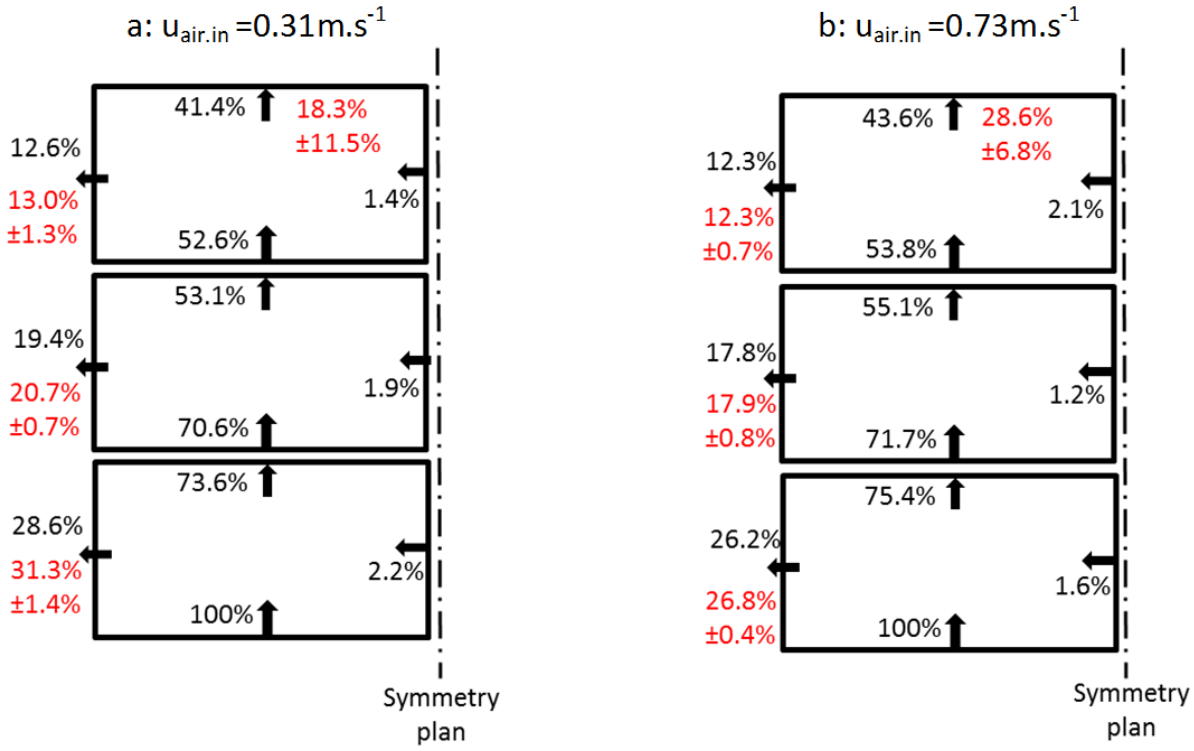

Figure 6. Distribution of the airflow rate (%) entering and exiting the cardboard box without heating (Q = 0W); numerical results (in black) and experimental results (in red): a) $u_{air.in}$ = 0.31 m.s^{-1}; b) $u_{air.in}$ = 0.73 m.s^{-1}

The experimental results are based on hot wire anemometer measurements. It can be seen that the model predicts very well the airflow rate through lateral vent holes for both upwind velocities. However, the difference became significant on the downstream face of the pallet. There are several reasons that lead to this uncertainty:

- The hot wire anemometer measures only one component of the velocity which could be different from the normal component used by the numerical model to compute the corresponding airflow rate. Therefore, the results depend greatly on the orientation of the velocity vector at the vent hole under consideration.
- The precision of the hot wire anemometer is 5% of the read value or ±0.03 $m.s^{-1}$, so it failed to measure the very low velocity that occurs in the downstream part of the pallet.
- The size of the hot wire anemometer is relatively large compared with the size of the vent holes, and can thus influence the airflow pattern.

For these reasons, the sum of these percentages given by the hot wire measurements on the external faces of the pallet is not equal to 100%.

When the product is heated, the airflow becomes more complex due to the occurrence of natural convection. Therefore, the hot wire anemometer measurements were not used to validate the model. Airflow measurements were performed using LDV.

The airflow measurements performed using LDV were carried out at the mid-height of the headspace (air gap between the product and the top of the carton). The measured and simulated dimensionless air velocities ($u_y/u_{air.in}$) are presented in Figure 7.

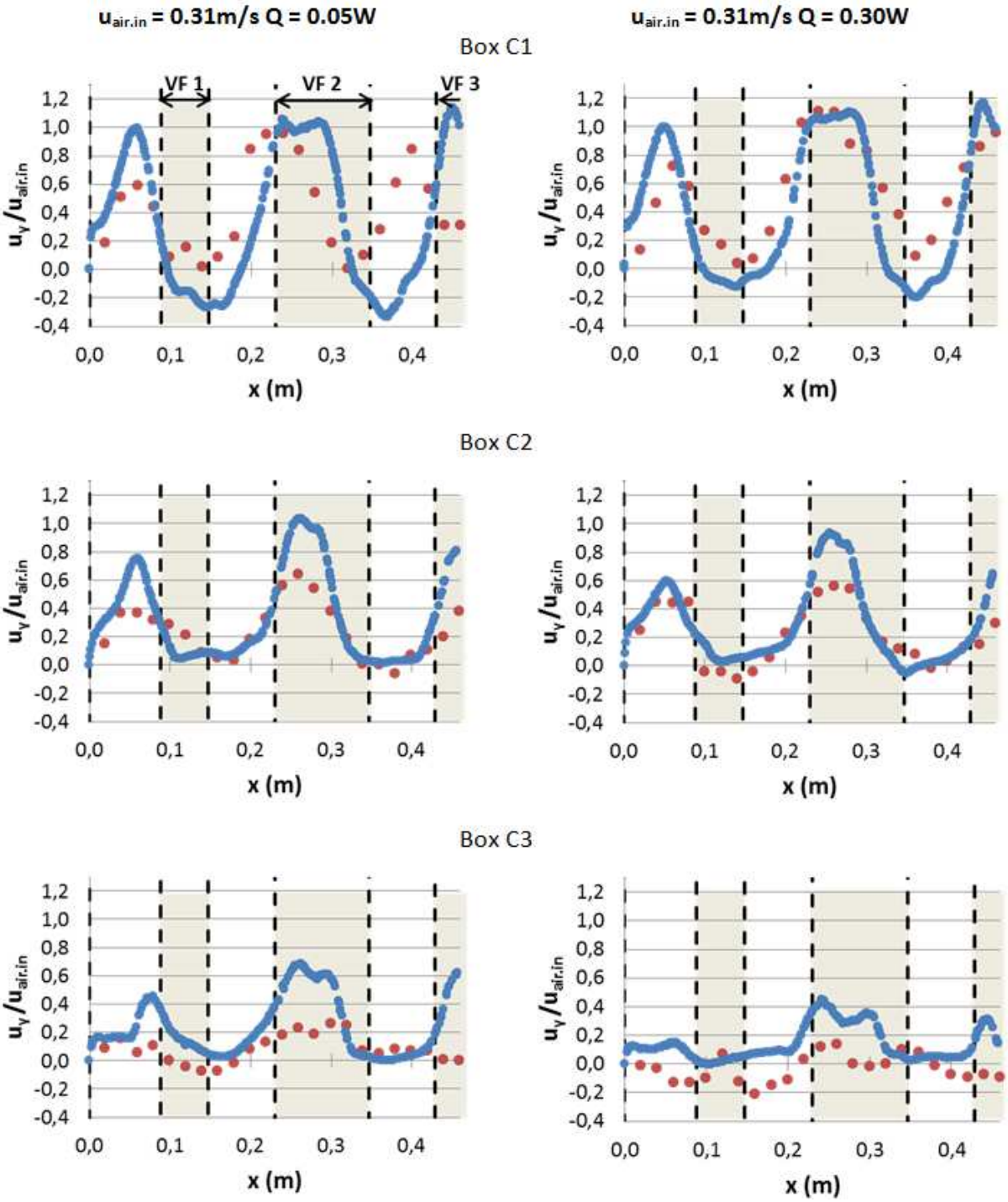

Figure 7. Comparison of the velocity transversal profiles in 3 boxes (C1, C2 and C3) where $u_{air.in}$ = 0.31 $m.s^{-1}$ and Q = 0.05 W (on the left) and 0.30 W (on the right): experiment (red dots), simulation (blue curve)

The results obtained using the model were consistent with the experimental results. It can be seen that the model allows prediction of the major airflow trends dominated by three velocity peaks related to the three vent holes VF1, VF2, VF3 (Figure 2).Numerical and experimental results show that the peaks in air velocity were not located at the center of the vent holes (VF1, VF2): they shifted to the left. This is due to the deviation in the airflow as it exits the pallet through the lateral vent holes. However, in the first box (C1), the maximum air velocity related to the VF2 jet is less deviated

than that of the VF1 jet. This can be explained by the fact that the surface of VF2 (16.2 cm^2) is twice that of VF1 and VF3 (8.2 cm^2). As the jet formed after exiting VF2 has a higher momentum flux (given by the flow rate multiplied by the velocity), it is more stable. The larger the vent hole area, the higher the air velocity in front of the hole.

Also, it can be observed that air slows down as it passes through the pallet. Numerical and experimental data show that the maximum velocity in the first box is of the same order of magnitude as the inflow air ($u_y/u_{air.in} \approx 1$). However, the numerical model under predicts the decay of the velocity ($u_y/u_{air.in}$) in boxes C2 and C3.

One of the explanations concerning the differences between the experimental and numerical results is that during the experiment, the products are not necessarily located at the same height and the surface of the packaging is not smooth. This increases the friction between fluid and walls. Therefore, the pressure drop in the head space was higher than predicted. Moreover, in the experiment, the products were not perfectly distributed inside the box. If two products touch each other, this may block the air circulation between them, implying the generation of a secondary vertical upward flow which can interact and slow down the main flow in the headspace. Also, the vent holes are not perfectly aligned which may decrease the area of the air passage implying higher pressure drops and thus lower velocities through vent holes separating packages.

Concerning the influence of heat generation on the velocities: similar profiles are observed in box C1 for Q = 0.05 W and 0.3 W. This clearly reflects the predominance of forced convection in the upstream part of the pallet where high velocities are observed. The main differences are observed in stagnant areas located downstream in boxes C2 and C3. Low but positive velocity areas are observed for Q = 0.05 W. However, high heat generation (Q = 0.30 W) gives rise to reverse flow with negative velocities which could be induced by secondary natural air circulation. We can observe that the numerical model fails to predict these local reverse flows associated with negative velocities which predominate in box C3 for Q = 0.30 W, where all predicted velocities have positive values.

The inability of the *k-ε* model to predict secondary reverse flows could be explained by the fact that it is more suitable for fully developed turbulence under steady state conditions for relatively high Reynolds values. However, in downstream boxes, stagnant areas associated with high heat generation (Q = 0.30 W) give rise to unsteady flow highly governed by thermal instabilities inherent in mixed convection regimes.

3.1.2 Temperature validation

The thermal validation of the model was performed using the temperature profile along one line of product at the center of the box (Figure 2) because this line was found to be representative of the distribution of the product temperature within the pallet (Pham et al., 2019). The profiles of the temperature difference with the incoming air ($\Delta T = T_p - T_{air.in}$) given by the model and the experiments are presented in Figure 8.

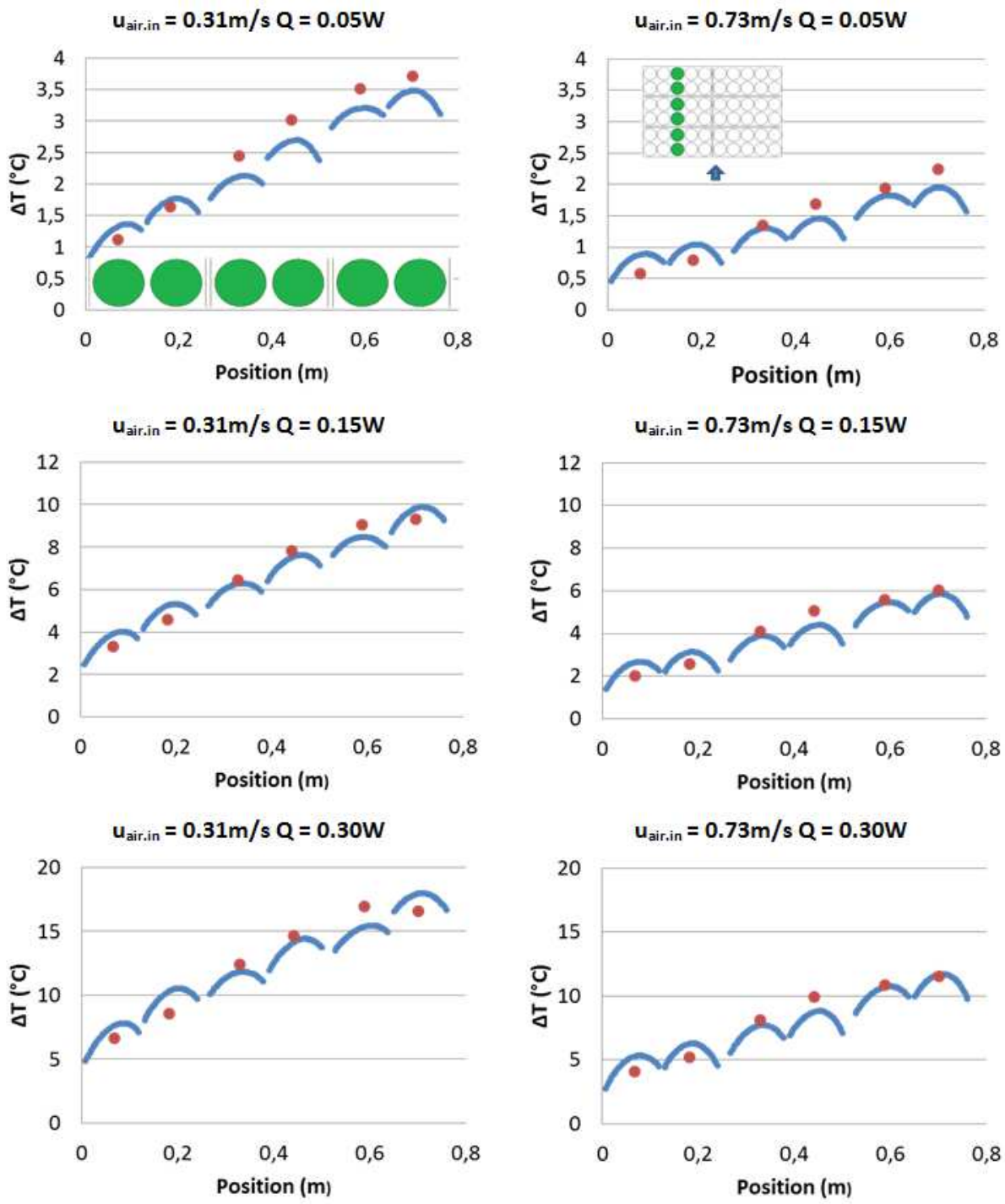

Figure 8. Comparison of the temperature profile in the center row of products with three heat fluxes and two upwind air velocities were chosen: Q = 0.05 W, 0.15 W and 0.30 W per 250-g product ; $u_{air.in}$ = 0.31m.s^{-1} and 0.73m.s^{-1}: experimental (red dots), simulation (blue curve)

The numerical results make it possible to obtain the temperatures along the diameter of the product (blue curve) and the experimental temperatures were measured at the center of the product (red dots. The local maximum temperature of one product is at its core as the temperature difference between the surface and the core of the product: the temperature difference is about 0.5°C when Q=0.05W and 2°C when Q=0.3W.

As expected, the greater the distance between the product and the ventilated surface, the higher the product temperature becomes. Overall, the model well predicted the trend as well as the temperature values. The maximum temperature difference between the model and the experimental value was less than 1.5°C in all cases.

3.2 Analysis of the numerical results

3.2.1 Airflow distribution

The contour of the pressure on 3 vertical plans passing by the center of the three vent holes is presented in the figure 9.

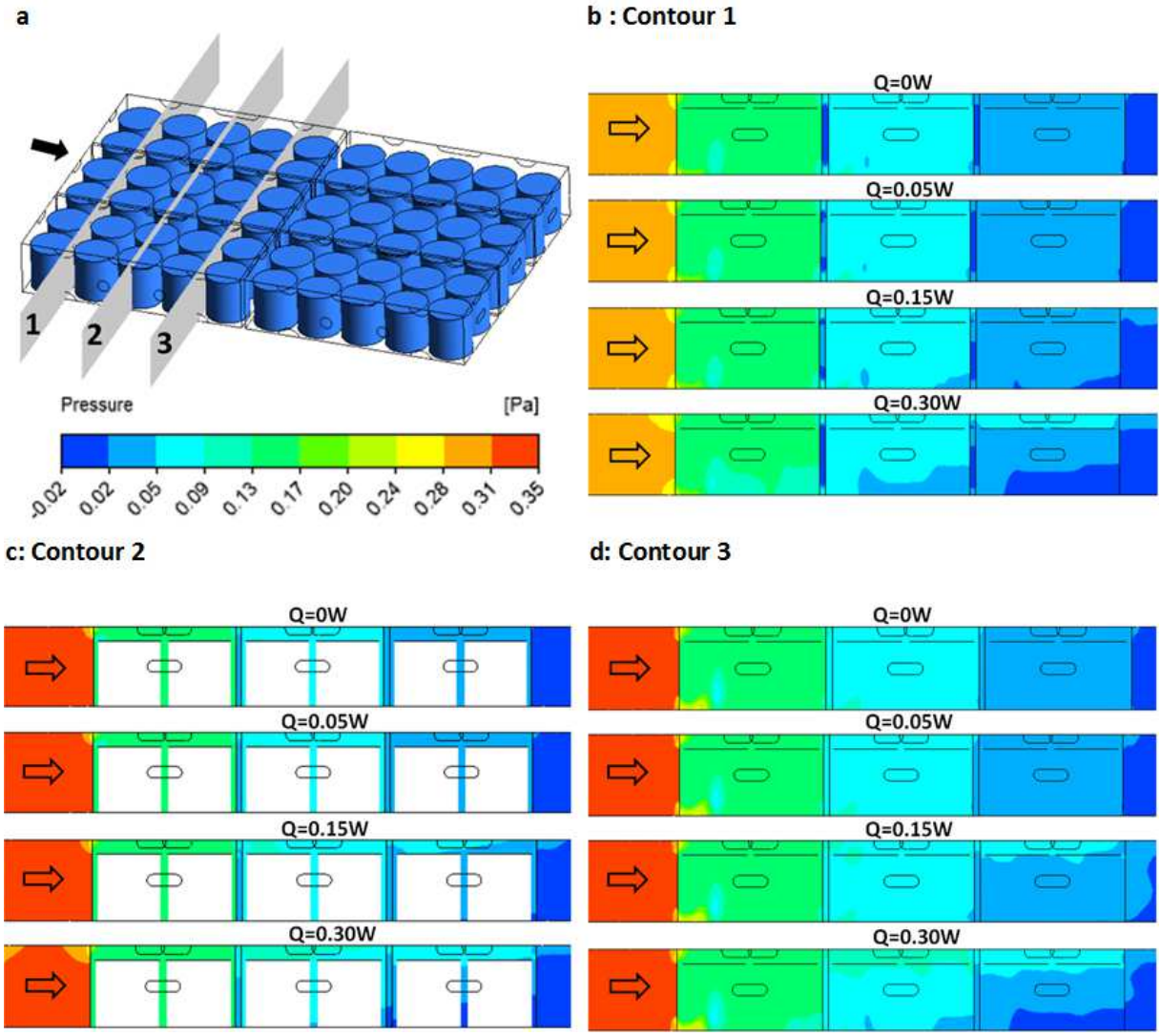

Figure 9 Vertical pressure contours where $u_{air.in}$=0.31m.s^{-1}: a) Positions of three contours; b, c, d correspond to contour 1, 2, 3 presented in a) respectively

The pressure just before entering the pallet is lower on the side of the pallet (contour 1) than at the center of the pallet (contour 2 and 3). This is due to the blockage effect of the pallet. The pressure decreases as air goes deeper into the pallet. However, the pressure field in each box is quite homogenous; the resistance of airflow due to products is negligible compared to that due to the vent holes. This is the case with the loosely packed products (Ambaw et al., 2017). The pressure drop due

to the product is more important for small and tightly packed product (Verboven et al. 2006). Except at the high heat flux (Q=0.30W), the pressure field in the first box is independent of the heat flux. However, starting from the end of the box C2 and especially in the box C3, the pressure balanced at the bottom with the outlet pressure. This suggests the entering of airflow due to natural convection at the bottom of box C3.

Figure 10 presents the contour of velocity at mid-height of the headspace air gap where $u_{air.in}$ = 0.31 $m.s^{-1}$.

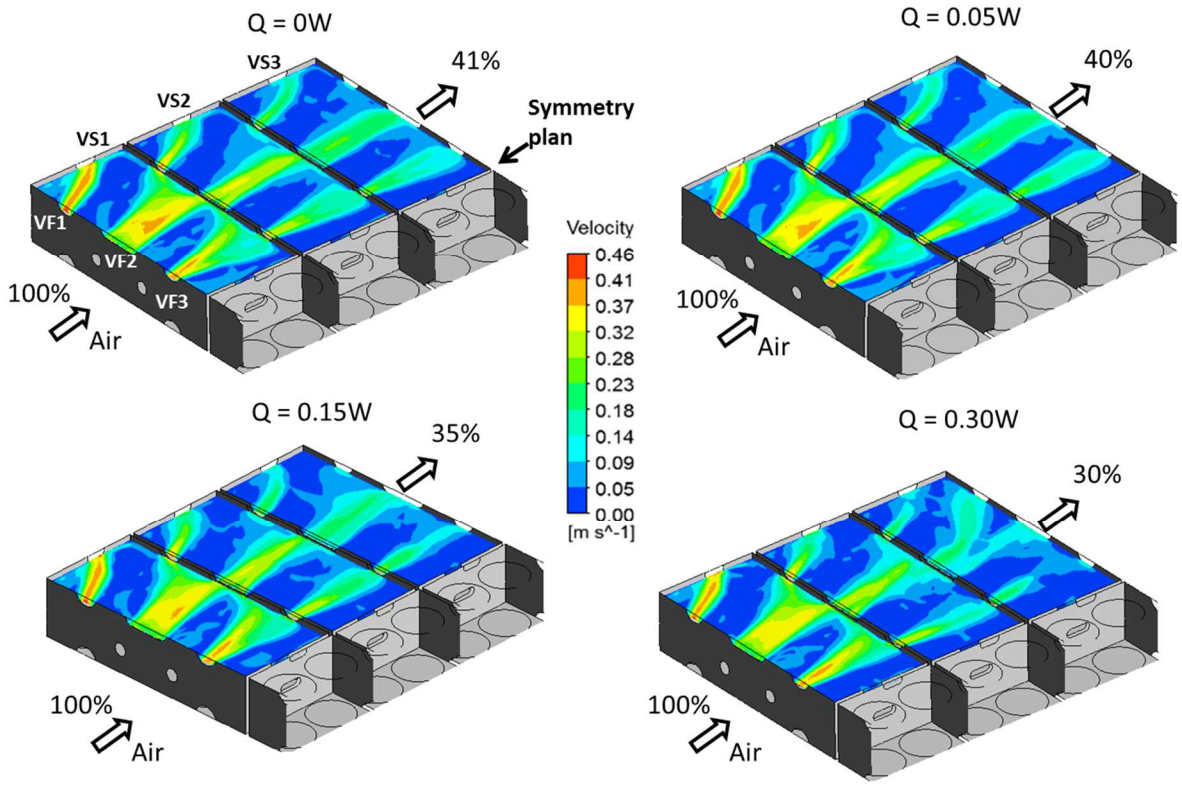

Figure 10. Velocity contours predicted by the model at the mid-height of the headspace air gap where $u_{air.in}$= 0.31 $m.s^{-1}$

Air entering by the three vent holes can be considered as three separate jets. The jet coming from the frontal vent hole VF1 is greatly influenced by the side vent hole (VS1), and is thus highly deviated. Most of air entering the box by the vent hole VF1 leaves the pallet through the side vent hole. The jets VF2 and VF3 were maintained to a greater extent since they were located further from the side wall of the pallet and thus allowed better internal ventilation of the whole pallet. Without heat flux (Q = 0 W) or low heat flux (Q = 0.05 W), the three jets become separated in the third box. However, when the heat flux is high (Q = 0.15 W and 0.30 W), the jets diffuse to a greater extent in the third box and mix together. These phenomena can also be observed through the air streamline (Figure 11). The airflow pattern in the third box (C3) changes significantly with the appearance of vertical airflow induced by natural convection.

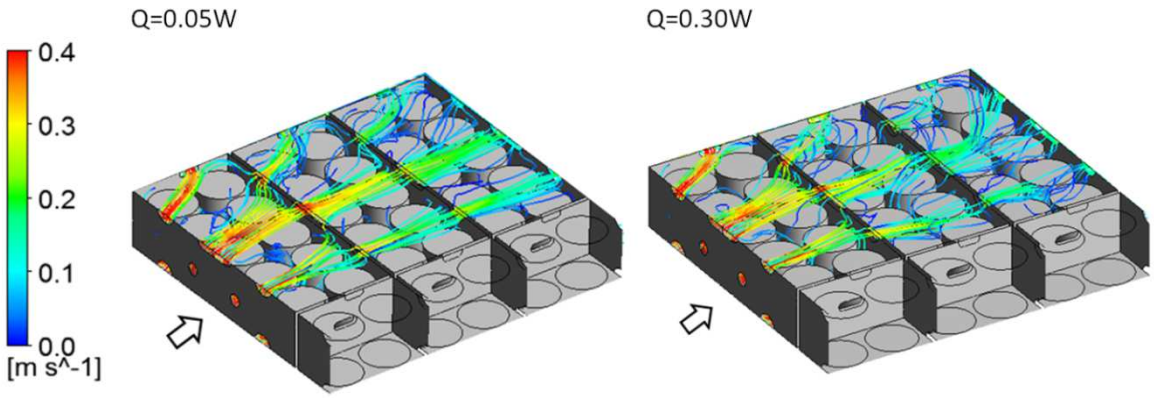

Figure 11 Air streamline passing through vent holes when $u_{air.in}$=0.31m.s^{-1}

Figure 12 presents air velocity vectors in a vertical plane in the third box (C3). This plane passes through the middle of the vent hole VF3 (Figure 2). The colour scale is based on the vertical component of the velocity.

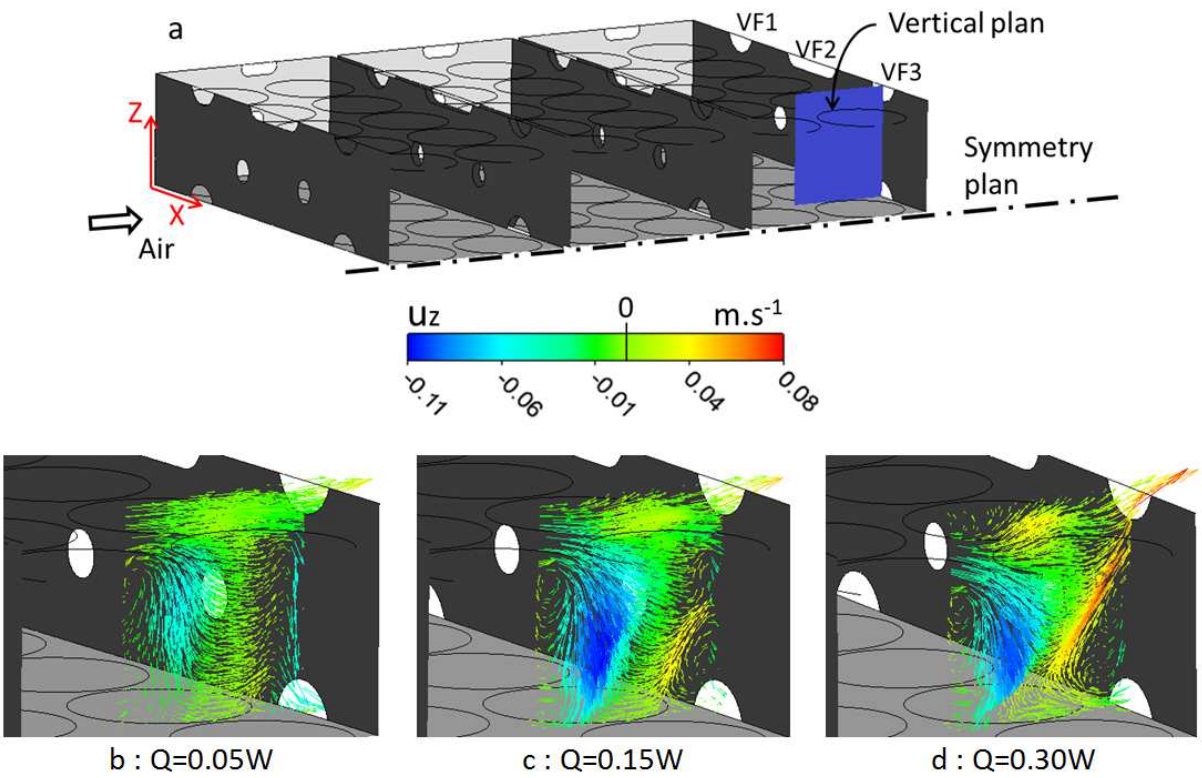

Figure 12. Air velocity vectors in a vertical plane in the third box $u_{air.in}$ = 0.31m.s^{-1}: a) position of the vertical plane; b: Q = 0.05 W; c: Q = 0.15 W ; d: Q = 0.30 W

It can be seen that when the heat flux is low (Q=0.05W), air exits the box via both the top and bottom vent holes and the vertical component of velocity is near zero. However, when the heat flux is higher (Q=0.15W), air starts to enter the box through the bottom vent hole. The amount of air entering the box increases when the heat flux increases (Q=0.30W), creating more active air circulation well within the box between the bottom and top holes. This confirmed the influence of natural convection in the third box.

3.2.2 Temperature distribution

Figure 13 presents the temperature profile at the mid-height of the product.

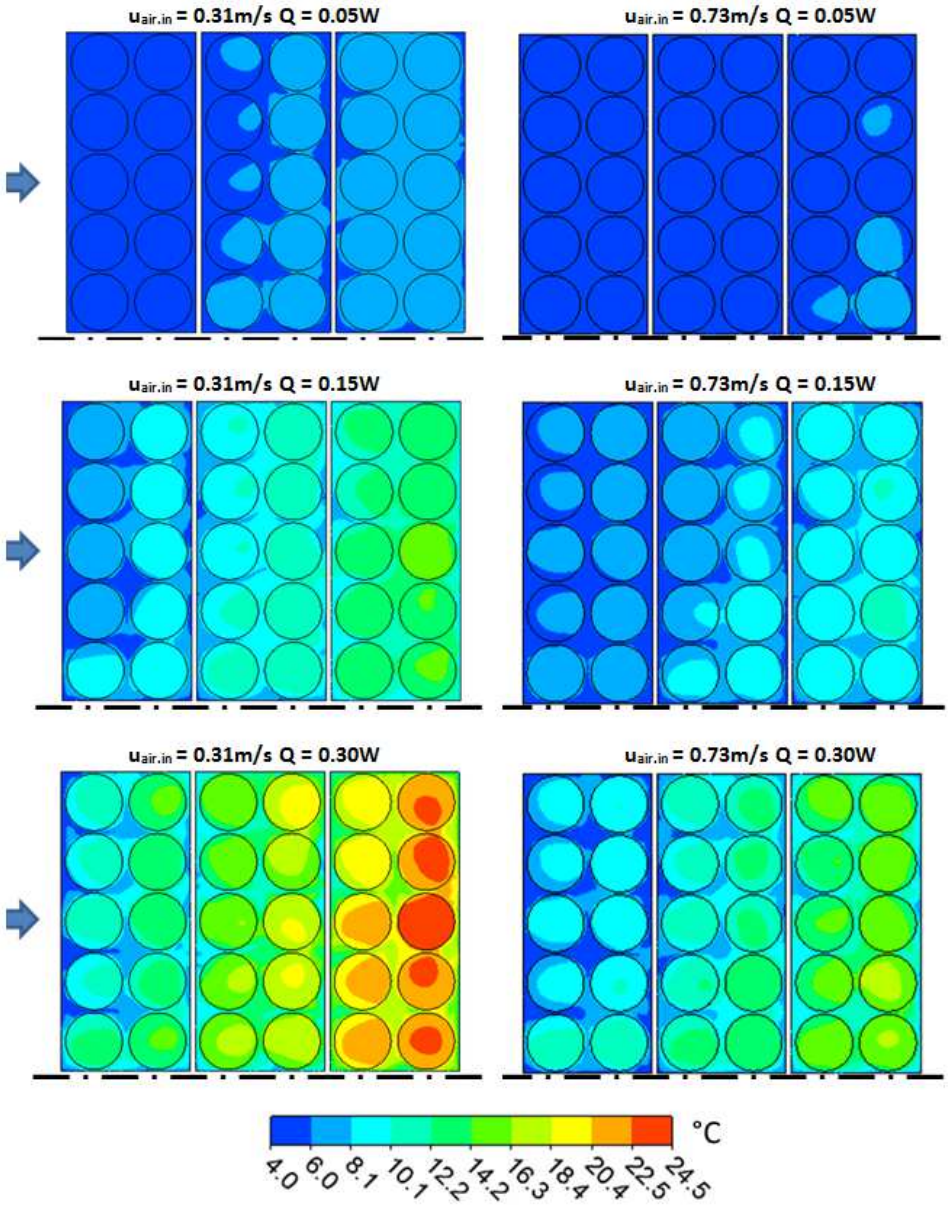

Figure 13. Temperature contours at the mid-height of the product.

Since air heats up and its velocity decreases as it passes through the pallet, the product temperature increases in the forced airflow direction. Obviously, the higher the heat flux and the lower the upwind air velocity, the higher the product temperature becomes. With the exception of the last row, the temperature of the product in a given row is quite uniform, and this trend could be explained by the relatively large opening area of 8.5% in this configuration.

When the heat flux is low (Q=0.05W), the hot spot (position of the highest temperature) is near the symmetry plane of the pallet. However, when the heat flux is high (Q=0.30W) the hot spot is located at the center product in the last row. This is because when natural convection is marked, air can enter the pallet through the bottom vent holes and these vent holes are not in the center of the box wall (Figure 2).

In order to evaluate the influence of natural convection on heat transfer, a simulation without taking into consideration gravity was carried out. Figure 14 presents the product temperature profiles with and without natural convection in the case Q=0.30W and $u_{air.in}$ = 0.31m.s^{-1}.

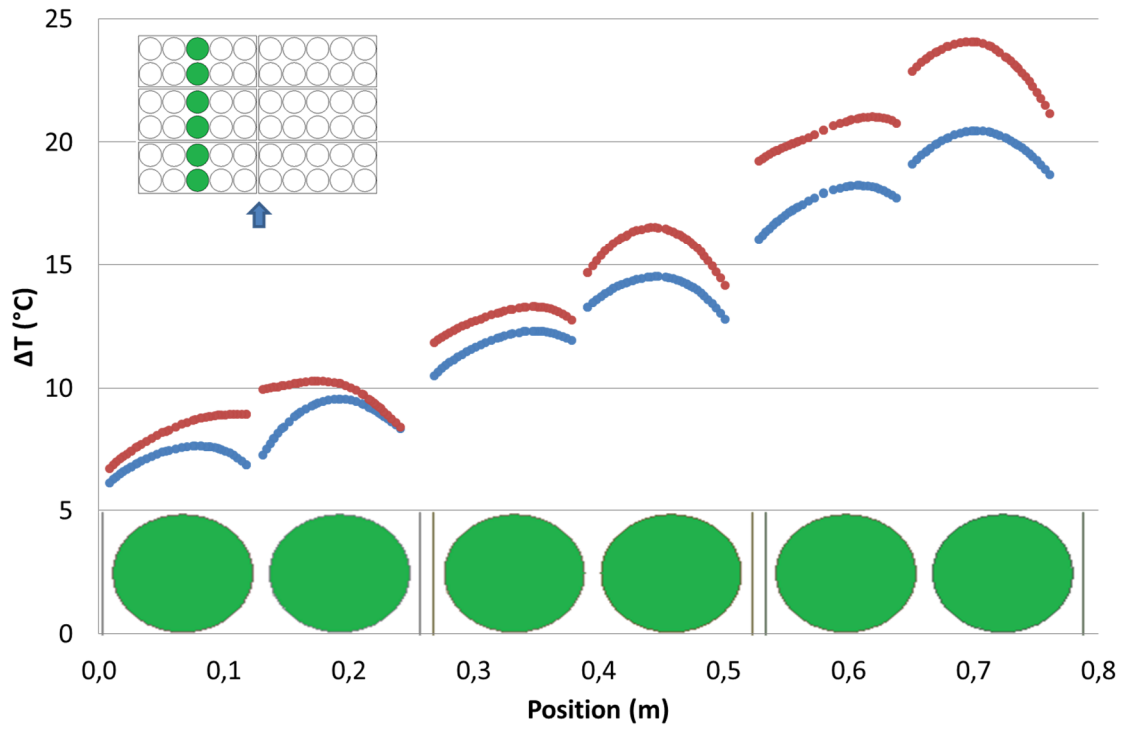

Figure 14. Comparison of the temperature profile in the center row of products (Q = 0.05 W, $u_{air.in}$ = 0.31 m.s^{-1}): with gravitation (natural convection) in blue and without gravitation in red

It can be seen that natural convection exerts a positive effect on heat transfer. The product temperatures are lower with natural convection. The deeper the product in the pallet, the greater the influence of natural convection (the higher the temperature difference between two simulations). This observation agrees with the results obtained by Bergman et al. (2011) indicating that buoyancy acts to enhance the rate of heat transfer associated with pure forced convection in transverse mixed convection (the forced flow is perpendicular to free flow).

4 Conclusion

In this study, experimental investigation and numerical simulation of a pallet of heat-generating product were carried out in order to characterize the distribution of the airflow and the product temperature within the pallet.

The model was validated by the experimental data. Satisfactory agreement was obtained for both air velocity and temperature profiles. The model predicted airflow distribution trends well.

A marked deviation of airflow was induced by the air loss through the lateral vent holes. Great heterogeneity of cooling was observed: the greater the distance of the products from the ventilated surface, the higher their temperatures became. Also, the higher the heat flux and the lower the air inflow velocity, the higher the product temperatures were.

This model can be used to study the influences of various pallet-related parameters, for example the area and the distribution of the vent holes. To simulate a case involving several pallets, the lateral boundary could also be modified. Moreover, it was possible to modify the arrangement of the boxes in a layer of the pallet, and also the ventilation axes.

5 Acknowledgements

We would like to acknowledge financial and technical supports for this work provided by CNIEL (the French Dairy Interbranch Organization) and ANRT (National Association of Research and Technology)

6 References

Ambaw, A., Delele, M.A., Defraeye, T., Ho, Q.T., Opara, L.U., Nicolaï, B.M., 2013. Verboven P., The use of CFD to characterize and design post-harvest storage facilities: Past, present and future. Computers and Electronics in Agriculture. 93, 184-194.

Ambaw, A., Bessemans, N., Gruyters, W., Gwanpua, S. G., Schenk, A., De Roeck, A., Delele, M. A., Verboven, P. and Nicolai, B. M., 2016. "Analysis of the spatiotemporal temperature fluctuations inside an apple cool store in response to energy use concerns." International Journal of Refrigeration. 66, 156-168.

Ambaw, A., M. Mukama, Opara, U.L., 2017. Analysis of the effects of package design on the rate and uniformity of cooling of stacked pomegranates: Numerical and experimental studies. Computers and Electronics in Agriculture. 136, 13-24.

Ali, R.K., H.A. Refaey, and M.R. Salem, 2018. Effect of package spacing on convective heat transfer from thermal sources mounted on a horizontal surface. Applied Thermal Engineering. 132, 676-685.

Asako, Y., Faghri, M., 1991. Parametric study of turbulent three-dimensional heat transfer of arrays of heated blocks encountered in electronic equipment. in American Society of Mechanical Engineers, Heat Transfer Division, (Publication) HTD.

Bergman, T.L., Lavine, A.S., Incropera, F.P., Dewitt, D.P., 2011. Introduction to heat trannsfer. sixth edition: Don Fowley.

Boutina, L., Bessaïh, R., 2011. Numerical simulation of mixed convection air-cooling of electronic components mounted in an inclined channel. Applied Thermal Engineering. 31(11), 2052-2062.

Castro, L.R., Vigneault, C., Cortez, L.A.B., 2004. Effect of container opening area on air distribution during precooling of horticultural produce. Transactions of the Asae. 47(6): p. 2033-2038.

Chong, D., Liu, J., Yan, J., 2008. Effects of duct inclination angle on thermal entrance region of laminar and transition mixed convection. International Journal of Heat and Mass Transfer. 51(15), 3953-3962.

Defraeye, T., Cronjé, P., Verboven, P., Opara, U. L., Nicolai, B., 2015. Exploring ambient loading of citrus fruit into reefer containers for cooling during marine transport using computational fluid dynamics. Postharvest Biology and Technology. 108, 91-101.

Defraeye, T., Lambrecht, R., Tsige, A. A., Delele, M. A., Opara, U. L., Cronjé, P., Verboven, P. and Nicolai, B., 2013. Forced-convective cooling of citrus fruit: Package design. Journal of Food Engineering. 118(1), 8-18.

Defraeye, T., Lambrecht, R., Delele, M. A., Tsige, A. A., Opara, U. L., Cronjé, P., Verboven, P. and Nicolai, B., 2014. Forced-convective cooling of citrus fruit: Cooling conditions and energy consumption in relation to package design. Journal of Food Engineering. 121, 118-127

Defraeye, T., Cronjé, P., Berry, T., Opara, U. L., East, A., Hertog, M., Verboven, P. and Nicolai, B., 2015. Towards integrated performance evaluation of future packaging for fresh produce in the cold chain. Trends in Food Science & Technology. 44(2), 201-225.

Dehghannya, J., Ngadi, M., Vigneault, C., 2012. Transport phenomena modelling during produce cooling for optimal package design: Thermal sensitivity analysis. Biosystems Engineering. 111(3), 315-324.

Delele, M.A., Tijskens, E., Atalay, Y. T., Ho, Q. T., Ramon, H., Nicolaï, B. M., Verboven, P., 2008. Combined discrete element and CFD modelling of airflow through random stacking of horticultural products in vented boxes. Journal of Food Engineering. 89(1), 33-41.

Delele, M. A., Ngcobo, M. E. K., Getahun, S. T., Chen, L., Mellmann, J. and Opara, U. L., 2013. Studying airflow and heat transfer characteristics of a horticultural produce packaging system using a 3-D CFD model. Part I: Model development and validation. Postharvest Biology and Technology. 86, 536-545.

Duret, S., Hoang, H. M., Flick, D., Laguerre, O., 2014. Experimental characterization of airflow, heat and mass transfer in a cold room filled with food products. International Journal of Refrigeration. 46, 17-25.

Ferrua, M.J. and R.P. Singh, 2008. A nonintrusive flow measurement technique to validate the simulated laminar fluid flow in a packed container with vented walls. International Journal of Refrigeration. 31(2), 242-255.

Ferrua, M.J. and R.P. Singh, 2009. Modeling the forced-air cooling process of fresh strawberry packages, Part I: Numerical model. International Journal of Refrigeration. 32(2), 335-348.

Getahun, S., Ambaw, A., Delele, D., Meyer,C.J., Opara, U.L., 2017. Analysis of airflow and heat transfer inside fruit packed refrigerated shipping container: Part II - Evaluation of apple packaging design and vertical flow resistance, Journal of Food Engineering. 203, 83-94.

Han, J.W., Zhao, C.J., Qian, J.P., Ruiz-Garcia, L., Zhang, X., 2018. Numerical modeling of forced-air cooling of palletized apple: Integral evaluation of cooling efficiency, International Journal of Refrigeration. 89, 131–141

Hélias, A., I.C. Trelea, and G. Corrieu, 2008. Assessment of respiratory activity during surface-mould cheese ripening. Journal of Food Engineering. 85(4), 632-638.

Hoang, M. H., Laguerre, O., Moureh, J., Flick, D., 2012. Heat transfer modelling in a ventilated cavity loaded with food product: Application to a refrigerated vehicle. Journal of Food Engineering. 113(3), 389-398.

Huang, Z., Z.-Y. Li, and W.-Q. Tao, 2017. Numerical study on combined natural and forced convection in the fully-developed turbulent region for a horizontal circular tube heated by non-uniform heat flux. Applied Energy. 185, 2194-2208.

Joye, D.D., 1996. Comparison of aiding and opposing mixed convection heat transfer in a vertical tube with Grashof number variation. International Journal of Heat and Fluid Flow, 1996. 17(2), 96-101.

Kader, B.A., 1981. Temperature and concentration profiles in fully turbulent boundary layers. International Journal of Heat and Mass Transfer. 24(9), 1541-1544.

Launder, B.E., Spalding, D.B., 1974. The numerical computation of turbulent flows. Computer Methods in Applied Mechanics and Energy. 3, 269–289.

Leclercq-Perlat, M.N., Sicard, M., Perrot, N., Trelea , I.C., Picque, D., Corrieu G., 2015. Temperature and relative humidity influence the ripening descriptors of Camembert-type cheeses throughout ripening. Journal of Dairy Science. 98(2): p. 1325-1335.

Maré, T., I. Voicu, and J. Miriel, 2005. Numerical and experimental visualization of reverse flow in an inclined isothermal tube. Experimental Thermal and Fluid Science. 30(1): p. 9-15.

Maughan, J.R., Incropera, F.P., 1987. Experiments on mixed convection heat transfer for airflow in a horizontal and inclined channel. International Journal of Heat and Mass Transfer. 30(7): p. 1307-1318.

Mohammed, H.A., Salman, Y.K., 2007a. Experimental investigation of mixed convection heat transfer for thermally developing flow in a horizontal circular cylinder. Applied Thermal Engineering. 27(8): p. 1522-1533.

Mohammed, H.A. and Y.K. Salman, 2007b. Combined convection heat transfer for thermally developing aiding flow in an inclined circular cylinder with constant heat flux. Applied Thermal Engineering. 27(8): p. 1236-1247.

Moureh, J. and D. Flick, 2004. Airflow pattern and temperature distribution in a typical refrigerated truck configuration loaded with pallets. International Journal of Refrigeration. 27(5): p. 464-474.

Moureh, J., Menia, N., Flick, D., 2002. Numerical and experimental study of airflow in a typical refrigerated truck configuration loaded with pallets. Computers and Electronics in Agriculture. 34(1–3): p. 25-42.

Moureh, J., Tapsoba, M., Flick, D., 2009. Airflow in a slot-ventilated enclosure partially filled with porous boxes: Part I – Measurements and simulations in the clear region. Computers & Fluids. 38(2): p. 194-205.

Ngcobo, M.E.K., Delele, M.A., Opara, U. L., Zietsman, C.J., Meyer C.J., 2012. Resistance to airflow and cooling patterns through multi-scale packaging of table grapes. International Journal of Refrigeration. 35(2): p. 445-452.

Ngcobo, M.E.K., Ngcobo, M. E. K., Delele, M. A., Opara, U. L. and Meyer, C. J., 2013. Performance of multi-packaging for table grapes based on airflow, cooling rates and fruit quality. Journal of Food Engineering. 116(2): p. 613-621.

O'Sullivan, J., Ferrua, M.J., Love, R., Verboven, P., Nicolaï, B., East, A., 2016. Modelling the forced-air cooling mechanisms and performance of polylined horticultural produce. Postharvest Biology and Technology. 120: p. 23-35.

Park, S.H., Kim, Y.H., Kim, Y.S., Park, Y.G., Ha, M.Y., 2018. Numerical study on the effect of different hole locations in the fan case on the thermal performance inside a gas oven range. Applied Thermal Engineering. 137: p. 123-133.

Pham, A.T., Moureh, J., Flick, D., 2019. Experimental characterization of heat transfer within a pallet of product generating heat. Journal of Food Engineering. 247: p. 115-125.

Sadashive Gowda, B., Narasimham, G.S.V.L., Krishna Murthy, M.V., 1997. Forced-air precooling of spherical foods in bulk: A parametric study. International Journal of Heat and Fluid Flow. 18(6): p. 613-624.

Sajadiye, S.M., Zolfaghari, M., 2017. Simulation of in-line versus staggered arrays of vented pallet boxes for assessing cooling performance of orange in cool storage, Applied Thermal Engineering. 115 337-349

Sarper, B., Saglam, M., Aydin, O., 2018. Experimental and numerical investigation of natural convection in a discretely heated vertical channel: Effect of the blockage ratio of the heat sources. International Journal of Heat and Mass Transfer. 126: p. 894-910.

Shih, T.-H., William W.L., Shabbir, A., Zhigang, Y., Zhu, J., 1995. A new k-ϵ eddy viscosity model for high Reynolds number turbulent flows. Computers & Fluids. 24(3): p. 227-238.

Sumon, S., Goutam, S., Mohammad, A., M. Quamrul, I., 2016. Combined free and forced convection inside a two-dimensional multiple ventilated rectangular enclosure. ARPN Journal of Engineering and Applied Sciences. Vol.1(No.1).

Tian, C., Wang, J., Cao, X., Yan, C., Ala, A.A., 2018. Experimental study on mixed convection in an asymmetrically heated, inclined, narrow, rectangular channel. International Journal of Heat and Mass Transfer. 116: p. 1074-1084.

Tutar, M., Erdogdu, F., Toka, B., 2009. Computational modeling of airflow patterns and heat transfer prediction through stacked layers' products in a vented box during cooling. International Journal of Refrigeration. 32(2): p. 295-306.

Van der Sman, R.G.M., 2002. Prediction of airflow through a vented box by the Darcy–Forchheimer equation. Journal of Food Engineering. 55(1): p. 49-57.

Verboven, P., Flick, D., Nicolaï, B.M., Alvarez, G., 2006. Modelling transport phenomena in refrigerated food bulks, packages and stacks: basics and advances. International Journal of Refrigeration. 29(6): p. 985-997.

Wu, W., Defraeye, T., 2018. Identifying heterogeneities in cooling and quality evolution for a pallet of packed fresh fruit by using virtual cold chains. Applied Thermal Engineering 133: 407-417.

Wu, W., Cronjé, P., Verboven, P., Defraeye, T., 2019. Unveiling how ventilated packaging design and cold chain scenarios affect the cooling kinetics and fruit quality for each single citrus fruit in an entire pallet, Food Packaging and Shelf Life. 21 100369.

Zhao, C.-J., Han, J.-W., Yang, X.-T., Qian, J.-P. and Fan, B.-L., 2016. A review of computational fluid dynamics for forced-air cooling process. Applied Energy. 168: p. 314-331.

Zou, Q., L.U. Opara, and R. McKibbin, 2006. A CFD modeling system for airflow and heat transfer in ventilated packaging for fresh foods: I. Initial analysis and development of mathematical models. Journal of Food Engineering. 77(4): p. 1037-1047.